Synergetic effects of NH_3 and NOx on the production and optical absorption of secondary organic aerosol formation from toluene photooxidation

Shijie Liu [a], Dandan Huang [b], Yiqian Wang [a], Si Zhang [a], Can Wu, Wei Du, Gehui Wang [a,c,*]

[a] Key Lab of Geographic Information Science of the Ministry of Education, School of Geographic Sciences, East China Normal University, Shanghai 210062, China

[b] State Environmental Protection Key Laboratory of Formation and Prevention of the Urban Air Pollution Complex, Shanghai Academy of Environmental Sciences, Shanghai 200233, China

[c] Institute of Eco-Chongming, Cuiniao Road, Chengjia Zheng, Shanghai 202150, China.

Corresponding author: Prof. Gehui Wang, e-mail: ghwang@geo.ecnu.edu.cn

Abstract

NH_3 is the most important alkaline gas in the atmosphere and one of the key species affecting the behaviors of atmospheric aerosols. However, the impact of NH_3 on secondary organic aerosol (SOA) formation remains poorly understood, especially the dynamic evolution of chemical compositions in the SOA formation process. A series of chamber experiments was performed to probe the individual and common effects of NH_3 and NOx on toluene SOA formation through OH-photooxidation. The chemical compositions of toluene SOA were characterized using the Aerodyne high-resolution time-of-flight aerosol mass spectrometer (AMS). From 637 ± 14.6 μg m^{-3} (control), the SOA mass concentration increased to 867 ± 12.7 μg m^{-3} in the presence of NH_3 and decreased to 452 ± 18.9 μg m^{-3} in the presence of NOx. However, the highest SOA concentration (1020 ± 10.6 μg m^{-3}) and the lowest carbon oxidation state (OS_C) occurred in the presence of both NH_3 and NOx, indicating that the higher volatility products that formed in the presence of NOx could precipitate into the particle-phase when NH_3 was added. This resulted in a synergetic effect on SOA formation when NH_3 and NOx co-existed. The heterogeneous reaction was the main pathway by which NH_3 participated in SOA formation in the photooxidation process. The synergetic effect of NH_3 and NOx was also observed in SOA optical absorption. A peak at 280 nm, which is characteristic of organonitrogen imidazole compounds, was observed in the presence of NH_3 and its intensity increased when NOx was added into the chamber. This work improves our understanding of how the synergistic interactions between NH_3 and NOx influence SOA formation and offers new insights into mitigating haze pollution.

Keywords: Photooxidation; Toluene; NH_3; Dynamic characteristics; Synergistic effects

1 Introduction

Secondary organic aerosols (SOA) are an important component of atmospheric particulate matter (Moise et al., 2015;Liu et al., 2017). SOA can significantly affect atmospheric visibility, air quality, and subsequently public health (Paciga et al., 2014;Yang et al., 2016;Liu et al., 2017). The optical properties of SOA have been directly and indirectly linked to their effects on the climate (Laskin et al., 2015;Xie et al., 2017;Peng et al., 2020). Because of the complexity of their chemical components, oxidation processes, and environmental factors, SOA formation mechanisms are very complex and the current understanding of SOA formation is incomplete. This limited understanding hampers the ability of models to predict the magnitudes, dynamics, and distributions of atmospheric aerosols from particulate and precursor emissions (Ortiz-Montalvo et al., 2014). In the past decades, although our understanding of SOA formation mechanisms has been constantly improving, there is still a gap between the simulated SOA concentration in large-scale atmospheric models and field observations (Volkamer et al., 2006;Yang et al., 2018).

Ammonia (NH_3) is the most important alkaline inorganic gas. It is widespread in the atmosphere and is one of the critical factors influencing SOA formation (Wang et al., 2016;Wang et al., 2018b;Chen et al., 2019). Some studies have noted that the presence of NH_3 can contribute to the formation of more aerosol mass through photooxidation (Na et al., 2007;Li et al., 2018). Na et al. (2007) observed that aerosol yields in the α-pinene-ozone oxidation system increased by 8% when NH_3 was added. Li et al. (2018) concluded that the presence of NH_3 in the aromatic hydrocarbon

photooxidation system increased aerosol size growth potentials (by 7%–108%), and resulted in enhanced SOA formation. Qi et al. (2020) found that the concentration and average diameter of SOA showed an immediate and rapid increase after adding NH_3. Furthermore, the acid-base reactions between NH_3/NH_4^+ and the carboxyl groups in SOA molecules might enhance SOA formation (Qi et al., 2020;Liu et al., 2015). The condensable ammonium salts formed from the reaction between NH_3 and organic acids reduce the volatility of the organic acids by several orders of magnitude (Paciga et al., 2014), and act as particle-phase organics that further promote SOA formation (Na et al., 2007;Huang et al., 2012;Chen et al., 2019;Qi et al., 2020;Wu et al., 2020). Along another pathway, carbonyls can undergo nucleophilic attack by NH_3 through the Maillard reactions and form the corresponding iminium intermediates (Noziere et al., 2009;Laskin et al., 2015;Liu et al., 2015). The iminium intermediates can continue to react with carbonyls, which activates further transformations such as the formation of heterocyclic compounds and oligomerization reactions and forms condensation (oligomeric) products with more stable secondary imines (Schiff bases) (Laskin et al., 2014). Both Noziere et al. (2009) and Ortiz-Montalvo et al. (2014) reported NH_3 is an efficient catalyst for reactions with carbonyl compounds to form nitrogen-containing organic aerosols (NOA). The reaction between carbonyl and NH_3 can significantly decrease the volatility of oxidation products, which further increases the yield of SOA (Lee et al., 2013;Zhang et al., 2015a;Qi et al., 2020). Babar et al. (2017) found that the substantial formation of secondary imines in the presence of NH_3 was responsible for the higher α-pinene SOA yields. However, not all studies have shown that the presence

of NH_3 increases SOA yields. One study observed that NH_3 suppressed SOA formation under certain ozonation conditions (Ma et al., 2018b). Furthermore, the consumption of NH_3 by Criegee intermediates was reported to decrease the secondary ozonide yield and thus affect SOA formation.

Nitrogen oxides (NOx = NO + NO_2), which are mainly emitted from the combustion of fossil-fuels, have received significant attention due to their effects on the photooxidation process of volatile organic compounds (VOCs) and SOA formation (Surratt et al., 2006;Ng et al., 2007b;Draper et al., 2015;Berkemeier et al., 2016;Sarrafzadeh et al., 2016;Zhao et al., 2018). A clear increase at first and then a decrease in the SOA yield was found with increasing NOx concentration from the laboratory experiments with both artificial (trimethylbenzene) and biological (β-pinene) VOCs (Sarrafzadeh et al., 2016;Yang et al., 2020). The competitive chemistry of organic peroxyl radicals (RO_2) with hydroperoxyl radicals (HO_2) and NO was responsible for the variability in SOA formation (Ng et al., 2007a;Xu et al., 2014;Jiang et al., 2020). RO_2 mainly reacts with HO_2 under low-NOx conditions to form oxidation products with lower volatility, which may enable it to precipitate into the particle-phase and contribute to the SOA mass (Ng et al., 2007a). While the RO_2 + NO reaction is dominant in high-NOx conditions, the increase in volatile products formed through fragmentation was responsible for the decrease in SOA yield with increasing NOx (Zhao et al., 2018;Liu et al., 2019a;Xu et al., 2020). In addition, the increase of OH concentration formed through NO + HO_2 →NO_2 + OH reaction at low-NOx conditions, and a suppressing effect of NOx on OH formation under high-NOx conditions was

partly responsible for the first increasing and then decreasing trend of SOA yield with NOx concentration (Sarrafzadeh et al., 2016;Bates et al., 2021).

In the last decade, atmospheric pollutants in China have changed significantly in their concentrations and composition (Wang et al., 2015;Xia et al., 2016) with the emissions of SO_2 and NOx decreased by 75% from 2007–2015 and 10% from 2011–2015, respectively (de Foy et al., 2016;Vu et al., 2019;Wang et al., 2020). However, owing to the lack of regulation regarding NH_3 emissions, NH_3 emissions increased by ~30 % from 2008–2016 over the North China Plain (Liu et al., 2018). As has been pointed out in previous research, the promoting effect of NH_3 on the formation of SOA may counteract the decreases in aerosol formation due to reductions in SO_2 and NOx (Zhang et al., 2021a). Indeed, field observation and model simulation have pointed out that the reduction of NH_3 emissions contribute much to the improvement of $PM_{2.5}$ pollution compared to SO_2 in winter (Erisman and Schaap, 2004). Hence, the mechanism by which NH_3 affects SOA formation has attracted more and more attention (Wang et al., 2018a;Ge et al., 2019;Zhang et al., 2021b). However, previous studies have not paid sufficient attention to the joint impacts of NH_3 and NOx on the formation of SOA and its corresponding optical properties. Due to the lack of real time detection methods for SOA chemical composition, the dynamic characteristics of how NH_3 participates in SOA formation via photooxidation have not been extensively studied.

Toluene is one of the most abundant aromatic VOCs in the urban atmosphere, which is also an important source of brown carbon (Laskin et al., 2010;Ma et al., 2018a). The effects of NH_3 and NOx on SOA formation through the toluene photooxidation

process were investigated in this study. The chemical composition of toluene SOA was characterized on-line with an aerosol mass spectrometer and the characteristics of SOA chemical composition under different conditions were further explored by applying a positive matrix factorization (PMF) analysis. The optical properties of toluene SOA particles were determined based on a UV-vis spectrum analysis. Possible mechanisms of the effects of both NH_3 and NOx on SOA formation were discussed. The results will help us to better understand SOA formation mechanisms in complex pollution conditions with elevated NH_3 and NOx concentrations in an urban atmospheric environment.

2 Materials and Methods

2.1 Photooxidation chamber experiments

All toluene photooxidation experiments were performed in a 4 m^3 chamber. The chamber has been described in detail in our previous study (Liu et al., 2021). Briefly, the chamber was constructed with a 0.08 mm-thick FEP-Teflon film. 50 UV-B lamps (TUV36W, Philips) with peak wavelengths of 254 nm were set up around the chamber and used as the light source to drive OH radical formation through hydrogen peroxide (H_2O_2) photolysis. Mirror surfaced stainless steel was used as the interior wall of the enclosure to maximize and homogenize the interior light intensity. All experiments were performed at room temperature (293~298 K) and one atmospheric pressure was maintained in the chamber at all time.

Before each experiment, the chamber was flushed with zero air for at last 18 hours, after which the concentration of particles was less than 1 cm^{-3}. Zero air was generated by a zero air supply (111-D3N, Thermo Scientific^{TM}, USA). The flow rate of zero air was controlled at 20 L min^{-1} by a mass flow controller (D088C/ZM, Beijing Sevenstar Electron Corporation) during the process of inflating. The relative humidity (RH) of zero air was about 20%. For each experiment, measured amounts of toluene (Sigma-Aldrich, analytically pure) and H_2O_2 solution (Sigma-Aldrich, 30 wt% in H_2O) were injected into a Teflon bulb with micro syringes. Zero air was passed through the injection tube to make sure all the liquids had evaporated to the gas-phase and were blown into the chamber. Toluene concentration was measured with a Proton Transfer Reaction-Mass Spectrometry (PTR-ToF-MS, Ionicon Analytik, Austria). The evolution of toluene concentration for different experiments was shown in Fig. S1. The OH concentration in the chamber was calculated based on the first order decay of toluene concentration. There was no obvious difference of OH concentrations in the different NOx and NH_3 levels (Fig. S2). The average OH concentration over the entire reaction period was 5.87×10^7 molecule cm^{-3}. NOx (Air Liquid Shanghai, 510 ppm NO_2 in N_2) and/or NH_3 (Air Liquid Shanghai, 502 ppm NH_3 in N_2) were introduced directly into the chamber to reach the required concentrations. For experiments with NOx, although only NO_2 was introduced into the chamber before photooxidation, NO could be formed through NO_2 photolysis under the UV light irradiation, so NO always coexisted with NO_2 in the photooxidation system (Zhao et al., 2018). Each experiment was performed without seed aerosols. After all the reactants were added, the chamber stood quietly for

10 min without turning on the light to ensure that the reactant gases in the chamber were evenly mixed. The photooxidation started when the UV light was turn on.

The experimental conditions for the toluene photooxidation are listed in Table 1. In our work, the OH and toluene concentrations were higher than those of urban conditions. The purpose of the high OH and toluene concentrations is to obtain enough particle production samples for off-line collections and accurate measurements. The toluene concentrations remained stable under the different experimental conditions, the variation of toluene-derived SOA mass concentration and yield was only affected by the different NO_2 and/or NH_3 concentrations in this study. Toluene was studied here as the representative of total aromatic VOCs in the urban atmosphere. The concentration ratio of toluene to OH in this study is similar to that under the real atmospheric conditions (Prinn et al., 1995;Zou et al., 2015).

2.2 Particle concentration measurements

For each experiment, a scanning mobility particle sizer (SMPS) was used to record the particle size distribution and volume concentration of the toluene-derived SOA. The SMPS was composed of a differential mobility analyzer (DMA model 3081, TSI Inc., USA) and a condensation particle counter (CPC model 3776, TSI Inc., USA) which were used for screening particles with specific aerodynamic equivalent sizes (from 14.1 nm to 736.5 nm) and for counting the number of the selected particles, respectively. The sheath gas velocity was 3 L min^{-1} and the sample gas velocity was 0.3 L min^{-1}. The scan was repeated every 5 min. During each scan circle, the scan time was 240 s, and

the particle sizes ranged from 13.6 nm to 726.5 nm. A density of 1.4 g m^{-3}, which was measured by Ng et al. (2007), was used for the calculation of toluene SOA mass concentration from the particle volume concentration (Ng et al., 2007b).

2.3 Chemical characterization

In this study, the toluene SOA chemical compositions were characterized with an on-line high-resolution time-of-flight aerosol mass spectrometer (HR-ToF-AMS, Aerodyne Research Inc. USA). The sample flow passed through a Nafion dryer and the RH of the sample gas was reduced to below 20% before entering the AMS. In the injection port, an aerodynamic lens focused particles with a vacuum aerodynamic diameter below 1 μm into a narrow beam. Particles impacted a flash vaporizer (600°C) at the rear of the sizing region under high vacuum (~10^{-7} Torr) and were subsequently ionized by electron impact ionization (70 eV). Then, the positively charged ions entered the ToF section and were separated. V-mode (m/Δm = ~2000) was used in the AMS ToF section to achieve the high signal-to-noise ratio. The separated ion fragments were analyzed by a mass spectrometer with scans from 1 to 300 m/z. The composition-dependent collection efficiency (CE) was applied to the data based on the methods established by Middlebrook et al. (2012). For mass concentration calculations, 1.1, 1.2, and 1.4 were applied as the default relative ionization efficiency (RIE) values of nitrate, sulfate, and organic compounds, respectively. The standard AMS data analysis software SQUIRREL 1.63B coupled with PIKA 1.23B in the Igor Pro (WaveMetrics, Inc., Portland, Oregon), which were retrieved from http://cires1.colorado.edu/jimenez-

group/ToFAMSResources/ToFSoftware/, were used for the analysis of elemental ratios and the ion speciated compositions of toluene SOA in the chamber. Note that the elemental ratios (i.e., O/C, H/C, and N/C) and mass-to-carbon ratio (OM/OC) were all calculated using the Aiken-Ambient method for comparability with previous studies (Aiken et al., 2008). In order to further explore the changes in SOA chemical composition, a PMF of the high-resolution mass spectra was performed to determine the different organic aerosol (OA) factors during the toluene photooxidation process. We preformed the PMF analysis in the same way as Zhang et al. (2011), the details of which are provided in the Supporting Information.

2.4 Absorption measurements

The changes of absorption spectra and the absorbance of the toluene derived SOA under different conditions were determined using a UV spectrophotometer (UV-3600, Shimadzu, Japan) with a 1 cm cuvette. The SOA was collected from a 3 m^3 sample gas onto the 46.2 nm PTFE filter (Whatman™, UK). The collected SOA sample was dissolved in 5 mL of methanol (HPLC grade, > 99.8%) with 30 min of sonication. As reported by Chen and Bond (2010), > 92 % of SOA is extractable by organic solvents (e.g., methanol), which means that almost all organic matter was extracted in this study. The filter extracts were filtered through 0.2 μm PTFE syringe filters to remove suspended insoluble particles. Before detection of the optical absorbance, a cuvette filled with pure methanol was scanned as a blank to provide a spectral background. The absorption was detected over the range of 200 to 800 nm with a resolution of 0.5 nm^{-1}.

The light absorption coefficient of the particles at a specific wavelength λ (Abs_λ, M/m) was calculated according to Eq. R1:

$$Abs_\lambda=(A_\lambda-A_{700})\cdot\frac{V_l}{V_a\cdot L}\cdot\ln(10) \quad (R1)$$

where, A_{700} is the background value of light absorption intensity, calculated as the average value of light absorption intensity from 695–705 nm to reduce the limits of error in measurement; V_l and V_a are the volumes of methanol with dissolved particles and sampled air, respectively; and L is the optical path length. Because Abs_λ was strongly dependent on the amount of SOA, all Abs_λ results were normalized based on the SOA mass collected on the filter. The normalized result was defined as the mass absorption coefficient (MAC, $m^2\ g^{-1}$), calculated using Eq. R2:

$$MAC_\lambda=\frac{Abs_\lambda}{M} \quad (R2)$$

where, M ($\mu g\ m^{-3}$) represents the concentration of methanol-soluble organic carbon.

3 Result and Discussion

3.1 SOA formation

In order to investigate the effect of NH_3 and NOx on SOA formation from toluene photooxidation, a control test was carried out. SOA yield (Y) is defined as $Y = \Delta M_0/\Delta HC$, where ΔM_0 is the produced organic aerosol mass concentration ($\mu g\ m^{-3}$), and ΔHC is the mass concentration of reacted toluene ($\mu g\ m^{-3}$). The evolution of SOA mass concentrations and SOA yield at different conditions during the photooxidation process were shown in Fig. 1. Recent experiments shown that the wall loss of organic vapors to the Teflon walls should not be ignored (Zhang et al., 2014;Zhang et al.,

2015b), and represented a major challenge in investigating SOA formation with environmental chambers (Krechmer et al., 2020). The formation of SOA in laboratory chambers may be substantially suppressed due to losses of SOA-forming vapors to chamber walls, but this effects on SOA formation have not yet been quantitatively established. However, the particle wall loss rates were detected at the end of the chamber experiment after the UV-lamps were turned off, and the mass concentration was corrected with the same way of Jiang et al. (2020) and Pathak et al. (2007). After the wall loss correction, the particle mass concentration was almost constant, the different wall loss effect caused by gaseous oxidation products formed in the different experiment conditions was considered remedied. Interestingly, wall loss is increased 66% and 205% in Exp.2 (in the presence of NH3) and Exp.3 (in the mixed condition of NH_3 and NOx), respectively, when compared with the experiments with no NH_3 (Exp.1 and 4). The larger particle wall loss in the presence of NH_3 could be explained by increasing condensation process of oxidized organic vapors onto the Teflon chamber wall via oligomerization (for dicarbonyls) and ionic dissociation/acid-base reaction (for organic acids). There was a noticeable increase in the SOA mass concentration in the presence of NH_3, which was consistent with previous studies (Qi et al., 2020;Chu et al., 2016). The mass concentration of SOA increased from 637 ± 14.6 μg m^{-3} without NH_3 to a maximum of 867 ± 12.7 μg m^{-3} with 200 ppb NH_3. Previous studies attributed the enhancement of SOA to the formation of NOA from acid-base reactions between NH_3/NH_4^+ and carboxyl groups, or Maillard reactions of NH_3/NH_4^+ with carbonyl functional groups (Noziere et al., 2009;Ortiz-Montalvo et al., 2014;Liu et al., 2015;Qi

et al., 2020). In contrast, SOA concentrations were lower in the presence of NOx, and the maximum mass concentration of toluene SOA was only 452 ± 18.9 μg m^{-3} with 63 ppb initial NOx. The branching of RO_2 loss among different pathways has an important influence on the products distribution and SOA formation. The fate of RO_2 mainly depends on the concentrations of NOx (Zhao et al., 2018;Liu et al., 2019a;Xu et al., 2020). Numerous studies have shown that, instead of RO_2 reacting with RO_2/HO_2, NO would react with RO_2 to form the RO intermediate and produces more oxidation products with higher volatilities through fragmentation in the presence of NOx (Zhao et al., 2018;Liu et al., 2019a;Xu et al., 2020). Highly volatile compounds cannot readily partition into the particle-phase, so this substantially suppresses the formation of SOA.

The NOx and NH_3 had opposite effects on toluene SOA formation in this study. Interestingly, however, the highest SOA mass concentration (1020 ± 10.6 μg m^{-3}) occurred in the presence of both NOx and NH_3, which was nearly 1.6 times higher than that observed with no NOx or NH_3. Although inorganic aerosol was formed from the interaction of NH_3 and NOx in the chamber, the upper limit of the inorganic matter only account for 6.6% of the total mass of particulate matter (Table S1) in the NH_3 + NOx experiment. Therefore, it was not the main cause of the increase in particulate matter. Therefore, together NH_3 and NOx had a synergistic effect on SOA formation because their combined effect on SOA formation was greater than the sum of their separate effects. Qi et al. (2020) observed the promotion of NH_3 on toluene SOA formation was more obviously under high NOx concentration, SOA yield increased 3.7% and 4.6% for 70 ppb and 160 ppb initial NOx concentration, respectively, when 200 ppb NH_3 was

added into the chamber. Li et al. (2018) showed that the presence NH_3 can promote the particle size growth of SOA; at the same time, this particle growth rate was higher under low VOC/NOx (or high NOx) conditions. All in all, the joint effect of multiple environmental factors on SOA formation is not the simple summation of the influences of various factors on SOA formation. This may at least partly explain why predictions of SOA concentrations in large-scale atmospheric models, which typically describe SOA formation from data derived from chamber experiments, are frequently lower than field observations (Volkamer et al., 2006).

3.2 SOA chemical composition

The traditional SOA formation mechanism is based on the chemical compositions obtained through off-line detection of the chemical composition of SOA (Jang et al., 2002;Liu et al., 2019a;Xu et al., 2020). SOA is continually evolving in the atmosphere and the ageing process of SOA co-occurs with its formation process, resulting in the transformation of SOA chemical composition continuously proceeding during the photooxidation process, but little attention has been paid to the evolution of SOA chemical composition in previous studies. Therefore, the AMS was used for on-line measurement of the SOA chemical composition and how the chemical composition evolved in the photooxidation process would be discussed in this section below.

Chemical composition of SOA is very complex. The average carbon oxidation state (OS_C) has been shown to be an ideal conceptual framework to describe changes in the degree of oxidation undergone by SOA (Kroll et al., 2011), and has been widely

applied in field and laboratory studies (Chen et al., 2018;Mandariya et al., 2019). Average OS_C calculation was shown in Supporting Information. Fig. 2 shows the changes in the OS_C of toluene SOA formed in different experiments. Notably, toluene SOA OS_C values was in the range between -0.5 and 0, which is consistent with that of semi-volatile oxygenated organic aerosols (SV-OOA). However, the different OS_C values and the change trends observed for the toluene SOA formed in different conditions (with and without NH_3/NOx) in Fig. 2 indicated that there was a photooxidation mechanism active during SOA formation, which ultimately changed the SOA chemical compositions.

The OS_C increased over time for all SOAs that were formed in the absence of NH_3. There are several possible reasons for the increasing trend of OS_C values. Firstly, a dynamic equilibrium of semi-volatile vapors may have been achieved between the particle-phase and gas-phase during the earlier toluene oxidation process. The increase of SOA led to a reduction in the concentration of gas-phase semi-volatile organic products. A decreasing concentration of gas-phase semi-volatile organic compound products would suppress their transformation from gas-phase to particulate-phase. More lower volatility gas-phase oxidation products with higher OS_C values would then be shifted to the particle phase, which would be responsible for the continuing increase of SOA and its OSc. Secondly, the formed SOA could have further been oxidized by OH radical through heterogeneous reactions (Kourtchev et al., 2015;Liu et al., 2019b). This could be the main reason for the increase in the OS_C when the SOA concentration was no longer increasing. Finally, as pointed by Malecha and Nizkorodov (2016), even

346 if there was no OH radical in the chamber, the photodegradation of SOA can produce
347 small oxygenated volatile organic compounds (e.g. acetaldehyde OS_C=-1, and acetone
348 OS_C≈-1.3) under UV light irradiation. The photoproduction of OVOCs from SOA had
349 a lower OS_C value than that of SOA. Although the loss of SOA through
350 photodegradation is small, the OS_C value of SOA still had increased to a certain extent
351 (Malecha and Nizkorodov, 2016).

352 The fact that additional photochemical processing results in the dynamic evolution
353 of the OS_C over time has been demonstrated in both field and laboratory experiments
354 (Jimenez et al., 2009). The atmospheric oxidation of OA tends towards higher OS_C
355 regardless of the original OA source (Herndon et al., 2008). However, when NH_3 was
356 present, the OS_C of total SOA went almost unchanged for the whole photooxidation
357 period. Carboxyl and carbonyl are the main oxygen-containing functional groups
358 responsible for the toluene photooxidation production (Ji et al., 2017). An organic
359 ammonium salt with four H atoms can offset an increase in OS_C value caused by the
360 formation of organic acids/carboxy group with two O atoms through acid-base reactions
361 (Kuwata and Martin, 2012;Liu et al., 2015). Or NH_3/NH_4^+ may react with carbonyl
362 functional groups through Maillard reactions, consuming the oxygen in the carbonyl
363 group and leading to the formation of species with covalent carbon-nitrogen bonds (Lee
364 et al., 2013;Zhang et al., 2015a;Qi et al., 2020). Xu et al. (2018) showed that imidazole
365 compounds (OS_C ≈ -1.3) generated through heterogeneous reaction between NH_3 and
366 carbonyl compounds might contribute to the decrease in the OS_C of SOA. It is clear that
367 an increase in OS_C caused by the formation of oxygen-containing functional groups

(e.g., carboxyl, carbonyl, etc.) would be counteracted through acid-base reactions or Maillard reactions in the presence of NH_3. After 60 min of UV light irradiation, there was no more SOA formation; however, the OS_C did decrease slightly in Exp.2 and 3, illustrating that the NH_3 could continue to react with SOA through heterogeneous processes. Huang et al. (2016) also pointed out that the portion of semi-volatile products with low OS_C formed at the later stage of photooxidation also contributed to the decreased OS_C.

The OS_C of the toluene SOA formed with NOx was lower than that formed in the absence of NOx, no matter whether NH_3 was present in the chamber or not. This indicated that an increased NOx concentration benefits the formation high volatility oxidation products with lower OS_C values (Kroll et al., 2011;Jimenez et al., 2009). However, the relationships between OS_C and SOA mass concentration with and without NH_3 were the opposite of each other. Predictably, the SOA formation mechanism in the presence of NOx is different from that with NOx + NH_3. In the absence of NH_3, the RO intermediate, which is easily fragmented to produce relatively high-volatility compounds, was the dominant product of the NOx + RO_2 reaction (Zhao et al., 2018;Liu et al., 2019a;Xu et al., 2020). Highly volatile compounds cannot readily precipitate into the particle-phase, which subsequently results in a lower SOA yield in the presence of NOx (Yang et al., 2020). Thereby, both OS_C and the SOA mass concentration were lower when 60 ppb NOx was added into the chamber. However, when both NOx and NH_3 were present, the toluene derived SOA had the lowest OS_C value, but the highest mass concentration. This result suggested that although NOx promotes the formation

of higher volatility compounds. These higher volatility compounds (e.g. glyoxal) can react with NH_3 and precipitate into the particle-phase, which could contribute to the increase in SOA formation. Huffman et al. (2009) observed that aerosol volatility was inversely correlated with the extent of oxidation of OA components. The low value of OS_C in the presence of NOx indicated that NOx would promote the formation of the relatively high-volatility compounds. However, the lower OS_C value in the presence of NH_3 indicated that the high-volatility compounds would promote partitioning into the particle-phase when reacting with NH_3.

Fragments derived from the AMS data have also been widely used to explore the bulk compositions and properties of SOA (Ng et al., 2010;Ng et al., 2017). The m/z 43 (f43) frequency was dominated by ion $C_2H_3O^+$, which is the tracer for organic compounds with alcohol and carbonyl functional groups (Alfarra et al., 2006). Meanwhile, the m/z 44 (f44) signal was dominated by CO_2^+ ions, which is the tracer for organic compounds with carboxyl functional groups and indicator of highly oxygenated organic aerosols (Ng et al., 2010). Here, we use the approach of Ng et al. (2010) by plotting the fractions of the total organic signal at m/z 43 *vs.* m/z 44 (f43 *vs.* f44). The change of f43 *vs.* f44, which has an inflection point during the photooxidation process, is shown in Fig. 3 and Fig. S3. In our study, the change before the inflection point was defined as the formation stage, and the linear fit of f43 *vs.* f44 for the formation stage is shown by the dashed lines. The change in f43 *vs.* f44 after the inflection point was defined as the stable stage, and the linear fit of f43 *vs.* f44 in this stage is shown by the solid lines. The formation and stable stages of the f43 *vs.* f44

412 relationship during the experiment are discussed separately here.

413 In the stable stage, the increase in f44 and decrease in f43 with increasing OH
414 exposure indicated that the carbonyl groups in toluene SOA were oxidized to carboxyl
415 groups by the ageing process. For the experiments without NH_3 and NOx, the slope
416 ratio of f43 *vs.* f44 was -3.9. When there was 60 ppb initial NOx, the f43 was almost
417 stable while the f44 increased with the oxidation process. There was a lower slope ratio
418 of f43 *vs.* f44, indicating that organic compounds with more alcohol and carbonyl
419 functional groups had formed in the presence of NOx. But for the experiments with 200
420 ppb initial NH_3, the slope ratios of f43 *vs.* f44 were only -1.1 and -1.3 in the presence
421 and absence of NOx, respectively. According to the above results, we can see that more
422 carbonyl groups are consumed as carboxyl groups are formed in the presence of NH_3.
423 The carbonyls can be oxidized to organic acids (Kawamura and Bikkina, 2016), but
424 extra-consumed carbonyls can be nucleophilically attacked by NH_3/NH_4^+ to form
425 nitrogen-heterocyclic compounds, e.g., imidazole (Grace et al., 2019;Lian et al., 2020).
426 Meanwhile, the peak f44 value decreased from 0.13 to 0.10 when NH_3 was added into
427 the chamber. This suggested that the heterogeneous reaction of NH_3/NH_4^+ could
428 promote the consumption of particle-phase carbonyl groups (Xu et al., 2018), and must
429 inhibit the formation of carboxyl groups in the SOA ageing process. According to the
430 changing trend of SOA concentration over time, the photooxidation process was
431 divided into formation stage and stable stage. As shown in Fig. 1, the first half hour of
432 photooxidation when SOA concentration increased linearly with time was defined as
433 SOA formation stage. After 60 min of photooxidation, SOA concentration was not

changed with reaction time, and it was defined as stable stage. The differences in spectra of toluene SOA in the formation stage and stable stage are shown in Fig. 4. A lower signal intensity variation of CO_2^+ in the presence of NH_3 also illustrated that NH_3 would inhibit heterogeneous reactions that form carboxyl groups.

In the formation stage, the slope ratios of f43 *vs.* f44 were almost the same for both experiments without NOx. It can thus be seen that the presence or absence of NH_3 does not affect the change trend of f43 *vs.* f44 in the SOA formation stage. Therefore, the gas-phase homogeneous reaction of NH_3 on SOA formation is not important. Clearly, the particle-phase heterogeneous reaction was the main reaction pathway by which NH_3 participated in the photooxidation process and toluene SOA formation. However, negative correlations were observed between f43 and f44 in the presence of NOx. Based on this, we concluded that NOx not only affects the SOA formation through the particle-phase heterogeneous reactions, but also through gas-phase homogeneous reactions.

3.3 PMF results

A temporal evaluation of the toluene SOA chemical composition during photooxidation is vital to the analysis of the NOA formation mechanism in the presence of NH_3 and/or NOx. Therefore, this study further compared the chemical properties of the SOA generated under different experimental conditions by applying a PMF analysis to the HR-ToF-AMS data (Chen et al., 2019). A summary of the PMF results is presented in Fig. S4-S7. For the toluene OH-photooxidation experiments with NH_3 and/or NOx presence, two factors were identified from the PMF analysis in the same

455 way of Chen et al. (2019). The H/C, O/C, and N/C values of these two factors are shown
456 in Fig. 5. The factor with higher N/C values was defend as high-nitrogen OA (Hi-NOA).
457 In contrast, the factor with lower N/C values was defend as low-nitrogen OA (Lo-NOA).
458 Fig. 6 exhibits the evolution of Hi-NOA and Lo-NOA during the photooxidation
459 process as resolved from the PMF analysis of different initial NOx/NH_3 concentrations.
460 While similar evolutionary trends were observed under different conditions, the relative
461 intensities and the chemical compositions of these two factors in each experiment were
462 not consistent.

463 For the toluene SOA formed under NH_3 conditions, both Lo-NOA and Hi-NOA
464 had similar O/C values, which were fully oxygenated with an average of 0.74 ± 0.04
465 (Fig. 5a). These O/C values were comparable to the low-volatility oxygenated organic
466 aerosols (LV-OOA) with an O/C value ranging from 0.6 to 1 (Jimenez et al., 2009). The
467 main difference between these two OA sources was the N/C ratio. The N/C ratio of Hi-
468 NOA (N/C = 0.032) was about three times higher than that of Lo-NOA (N/C = 0.010)
469 (Fig. 5a). The evolution of these two OA sources during the photooxidation process is
470 shown in Fig. 6a. The components of toluene SOA were mostly Lo-NOA during the
471 initial phase of SOA formation, but Hi-NOA toluene SOA started forming after 10
472 minutes and continued to increase. The Lo-NOA reached the maximum mass
473 concentration after 30 min of the photooxidation, and then decreased. Such a decline
474 trend of Lo-NOA at longer reaction times reflected the conversion of Lo-NOA into
475 something else in the particle-phase. As the Lo-NOA decreased, the mass concentration
476 of Hi-NOA gradually increased. Thus, the Hi-NOA should be derived from the

heterogeneous reaction of Lo-NOA with NH_3/NH_4^+. At the same time, it was proved that the formation pathway of Hi-NOA was not through reaction of NH_3 with later-generation gas-phase products in the homogeneous gas phase With the gradual replacement of Lo-NOA by Hi-NOA, the ratio of [Hi-NOA]/[Lo-NOA] stabilized at 5~6.

For the toluene SOA formed under NOx conditions, there was not a large difference between the N/C ratios of Hi-NOA (N/C = 0.019) and Lo-NOA (N/C = 0.014) (Fig. 5c). At the end of the NOx experiment, the ratio of [Hi-NOA]/[Lo-NOA] was only 3:2 (Fig. 6c). It follows that the contribution of the heterogeneous NOx reaction to the N/C ratio of toluene SOA was not obvious. Therefore, the formation of NOA in the presence of NOx mainly occurred through gas-phase homogeneous reactions, which was consistent with the results in section 3.3.

The changing trend of N/C with time in the presence of NH_3 was different to that with NOx present. The evolutions of the N/C of SOA in different experiments are shown in Fig. 7. In the presence of NH_3, the N/C value gradually increased throughout the photooxidation process. The increased N/C value in the photooxidation process was attributed to the heterogeneous NH_3 reaction with SOA. But in the presence of NOx, the N/C increased rapidly to its maximum value where it was stable for the rest of the reaction. This could mean that the heterogeneous reaction of toluene SOA with NOx to form NOA was not as important as the gas-phase homogeneous reaction.

When both NOx and NH_3 were added into the chamber, the N/C ratios of Hi-NOA and Lo-NOA were 0.062 and 0.029, respectively (Fig. 5b). The N/C ratio of Hi-NOA, which was comparable to the recently isolated nitrogen-enriched OA value (0.053) observed by Sun et al. (2011), was much higher than that observed in the experiments with only NH_3 or NOx. It was even higher than the sum of the N/C ratios from both Exp. 2 with NH_3 and Exp. 4 with NOx. In order to calculate the relative contributions of NH_3 and NOx to N/C, it was assumed that the effects of NH_3 or NOx on the N/C ratio in the Hi-NOA and Lo-NOA factors did not change among different experimental conditions. For Lo-NOA, the contributions of NH_3 and NOx to the N/C value were 0.0126 and 0.0164, and their relative intensities were 43% and 57%, respectively. While for the Hi-NOA, the contributions of NH_3 and NOx to the N/C values were 0.0404 and 0.0216, and their relative intensities were 65% and 35%, respectively. For the experiment with both NH_3 and NOx, the contribution of NH_3 to N/C was higher by 26%, and the contribution of NOx to N/C was higher by 17% compared to the experiments with single pollutants. The co-existence of NH_3 and NOx further enhanced the N/C value of toluene SOA, indicating that a synergetic interaction between NH_3 and NOx further enhanced organic nitrogen formation.

3.4 Optical absorption

The optical characteristics of toluene SOA formed from different NH_3 and NOx conditions were investigated. The MAC of toluene derived SOA detected over the range of 230–600 nm is displayed in Fig. 8. Over the entire UV detection range, an increase

518 in light absorption was observed when the toluene SOA formed in the presence of NOx
519 or NH_3.

520 By looking at Fig. 8 in detail, one can see that the MAC of toluene SOA formed
521 with (red line) and without (black line) NH_3 overlapped at 250 nm, but when the UV
522 wavelength exceeded 250 nm the MAC of the toluene SOA formed in the presence of
523 NH_3 was higher. The red line reflects an obvious characteristic absorption peak at
524 270~280 nm, which was mainly due to the absorption of the $n \rightarrow \pi^*$ electronic
525 transitions. The imidazole compounds were formed through the Maillard reactions
526 between NH_3/NH_4^+ with carbonyl functional groups (Zhang et al., 2015a). The C=N
527 double bonds in the organonitrogen imidazole compounds can act as effective
528 chromophores since both $\pi \rightarrow \pi^*$ and $n \rightarrow \pi^*$ transitions are chromatically active
529 (Nguyen et al., 2013). The UV/visible spectrum of imine and pyrrole show broad bands
530 at 270 nm (NIST, 2020), which was consistent with the UV absorption peak of the
531 $n \rightarrow \pi^*$ band observed here. According to the AMS results, carbonyl was the main
532 functional group of toluene SOA. The emergence of absorption peaks at 270~280 nm
533 demonstrated that some organonitrogen imidazole compounds (e.g. imines and pyrrole)
534 were formed through the heterogeneous reaction of toluene with NH_3. Meanwhile, the
535 high-molecular weight nitrogen-containing organic species might have formed through
536 Maillard reactions in the particle-phase (Wang et al., 2010). This was also a reason for
537 the increase in SOA mass concentration in the presence of NH_3.

538 The green line in Fig. 8 represents the MAC value of toluene-derived SOA in the
539 presence of NOx, which was also higher than the black line (control) throughout the

UV detection range. When compared with the red line, the green line had no obvious characteristic peak at 280 nm, but it had higher absorbance in the range between 240 and 280 nm. This indicated that both NOx and NH_3 increased the absorbance of toluene SOA, while the chromophores generated from the reactions between toluene-derived SOA with either NH_3 or NOx did not behave in the same way.

The blue line in Fig. 8 represents the absorbance of toluene SOA formed in the presence of both NOx and NH_3. The MAC of toluene SOA formed in the presence of both NOx and NH_3 was higher than the toluene SOA formed in the presence of either NH_3 or NOx. There might have been a synergetic effect between NOx and NH_3 on the absorbance of toluene SOA. Considering that the mass concentration of toluene SOA formed in the presence of both NH_3 and NOx was the highest, as described in section 3.1, the co-existence of NH_3 and NOx may also result in the toluene SOA having stronger light absorption and atmospheric radiative forcing. We also noted a higher MAC value at 280 nm, which illustrated that the presence of NOx could promote the formation of imines and pyrrole in the photooxidation system of toluene with NH_3.

4 Conclusion

Here we present the results of a study in which we characterized the mass concentrations, chemical compositions, and optical properties of SOA formed from the photooxidation of toluene under different NH_3 and NOx conditionsconcentrations. When compared with the control experiment, the SOA mass concentration data showed that the formation of toluene-derived SOA was enhanced in the presence of NH_3,

561 through acid-base reactions between carboxyl groups or Maillard reactions with
562 carbonyl compounds, but inhibited in the presence of NOx. Meanwhile, the mass
563 concentration of toluene SOA formed in the presence of both NOx and NH_3 was higher
564 than those formed under either NH_3 or NOx alone. This result indicated that there was
565 a synergistic interaction between NH_3 and NOx that further enhanced toluene-derived
566 SOA formation. At the same time, the lowest OS_C value was obtained when both NH_3
567 and NOx were present. We concluded that highly volatile compounds, which were
568 formed from toluene photooxidation in the presence of NOx, could react with NH_3 to
569 form products with lower volatilities, and promoted the partitioning of these products
570 into the particle-phase.

571 Synergetic effects of NH_3 and NOx on the formation of NOA and the optical
572 properties of SOA were also observed in this study. The heterogeneous reaction was
573 responsible for the formation of NOA in the presence of NH_3. Meanwhile, an absorption
574 peak at 270~280 nm, which is characteristic of imine and pyrrole, was observed. In
575 contrast, the formation of NOA caused by NOx alone was mainly due to a gas phase
576 homogeneous reaction.

577 In the actual atmosphere especially in Chinese urban atmosphere, NOx and NH_3
578 abundantly co-exist. Therefore, the findings presented here clearly show that the
579 synergetic effects of NOx and NH_3 should not be neglected. In the meantime, our work
580 provides a scientific basis for the consideration of synergistic emission reductions of
581 NH_3 and NOx under the compound pollution conditions, which will contribute to
582 reducing the burden of aerosols in the atmosphere. It has to be noted that the

concentration of reactants used for the experiments is much higher than that observed in polluted areas, the effect of NH_3 and NOx on the photooxidation of toluene with lower concentrations would be checked in the further study.

Data availability

The datasets are available upon request to the corresponding authors.

Author contributions

SL and GW designed the experiment. SL, DH and YW conducted the experiments. SL, DH, YW and GW performed the data interpretation. SL and GW wrote the paper. YW, SZ, CW, WD contributed to the paper with useful scientific discussions or comments.

Competing interests

The authors declare that they have no conflict of interest.

Acknowledgements

This work was financially supported by National Natural Science Foundation of China (Grant No. 42130704, 42005088); the China Postdoctoral Science Foundation (Grant No. 2019M661427); Fundamental Research Funds for the Central Universities, Director's Fund of Key Laboratory of Geographic Information Science (Ministry of Education), East China Normal University (Grant No. KLGIS2021C02); and ECNU Happiness Flower Program.

Reference

Alfarra, M. R., Paulsen, D., Gysel, M., Garforth, A. A., Dommen, J., Prevot, A. S. H., Worsnop, D. R., Baltensperger, U., and Coe, H.: A mass spectrometric study of secondary organic aerosols formed from the photooxidation of anthropogenic and biogenic precursors in a reaction chamber, Atmos. Chem. Phys., 6, 5279-5293, DOI 10.5194/acp-6-5279-2006, 2006.

Babar, Z. B., Park, J.-H., and Lim, H.-J.: Influence of NH_3 on secondary organic aerosols from the ozonolysis and photooxidation of α-pinene in a flow reactor, Atmos. Environ., 164, 71-84, 10.1016/j.atmosenv.2017.05.034, 2017.

Bates, K., Jacob, D., Li, K., Ivatt, P., Evans, M., Yan, Y., and Lin, J.: Development and evaluation of a new compact mechanism for aromatic oxidation in atmospheric models, Atmos. Chem. Phys. Discuss., 2021, 1-34, 10.5194/acp-2021-605, 2021.

Berkemeier, T., Ammann, M., Mentel, T. F., Poschl, U., and Shiraiwa, M.: Organic nitrate contribution to new particle formation and growth in secondary organic aerosols from α-pinene ozonolysis, Environ. Sci. Technol., 50, 6334-6342, 10.1021/acs.est.6b00961, 2016.

Chen, C. L., Li, L. J., Tang, P., and Cocker, D. R.: SOA formation from photooxidation of naphthalene and methylnaphthalenes with m-xylene and surrogate mixtures, Atmos. Environ., 180, 256-264, 10.1016/j.atmosenv.2018.02.051, 2018.

Chen, T. Z., Liu, Y. C., Ma, Q. X., Chu, B. W., Zhang, P., Liu, C. G., Liu, J., and He, H.: Significant source of secondary aerosol: formation from gasoline evaporative emissions in the presence of SO_2 and NH_3, Atmos. Chem. Phys., 19, 8063-8081, 10.5194/acp-19-8063-2019, 2019.

Chen, Y., and Bond, T. C.: Light absorption by organic carbon from wood combustion, Atmos. Chem. Phys., 10, 1773-1787, 10.5194/acp-10-1773-2010, 2010.

Chu, B. W., Zhang, X., Liu, Y. C., He, H., Sun, Y., Jiang, J. K., Li, J. H., and Hao, J. M.: Synergetic formation of secondary inorganic and organic aerosol: effect of SO_2 and NH_3 on particle formation and growth, Atmos. Chem. Phys., 16, 14219-14230, 10.5194/acp-16-14219-2016, 2016.

de Foy, B., Lu, Z., and Streets, D. G.: Satellite NO_2 retrievals suggest China has exceeded its NOx reduction goals from the twelfth Five-Year Plan, Sci. Rep., 6, 35912, 10.1038/srep35912, 2016.

Draper, D. C., Farmer, D. K., Desyaterik, Y., and Fry, J. L.: A qualitative comparison of secondary organic aerosol yields and composition from ozonolysis of monoterpenes at varying concentrations of NO_2, Atmos. Chem. Phys., 15, 12267-12281, 10.5194/acp-15-12267-2015, 2015.

Erisman, J. W., and Schaap, M.: The need for ammonia abatement with respect to secondary PM reductions in Europe, Environ. Pollut., 129, 159-163, 10.1016/j.envpol.2003.08.042, 2004.

Ge, S., Wang, G., Zhang, S., Li, D., Xie, Y., Wu, C., Yuan, Q., Chen, J., and Zhang, H.: Abundant NH_3 in China enhances atmospheric HONO production by promoting the heterogeneous reaction of SO_2 with NO_2, Environ. Sci. Technol., 53, 14339-14347, 10.1021/acs.est.9b04196, 2019.

Grace, D. N., Sharp, J. R., Holappa, R. E., Lugos, E. N., Sebold, M. B., Griffith, D. R., Hendrickson, H. P., and Galloway, M. M.: Heterocyclic product formation in aqueous brown carbon systems, ACS Earth Space Chem., 3, 2472-2481, 10.1021/acsearthspacechem.9b00235, 2019.

Herndon, S. C., Onasch, T. B., Wood, E. C., Kroll, J. H., Canagaratna, M. R., Jayne, J. T., Zavala, M. A., Knighton, W. B., Mazzoleni, C., Dubey, M. K., Ulbrich, I. M., Jimenez, J. L., Seila, R., de Gouw, J. A., de Foy, B., Fast, J., Molina, L. T., Kolb, C. E., and Worsnop, D. R.: Correlation of secondary organic aerosol with odd oxygen in Mexico City, Geophys. Res. Lett., 35, Artn L15804, 10.1029/2008gl034058, 2008.

Huang, D. D., Zhang, X., Dalleska, N. F., Lignell, H., Coggon, M. M., Chan, C. M., Flagan, R. C., Seinfeld, J. H., and Chan, C. K.: A note on the effects of inorganic seed aerosol on the oxidation state of secondary organic aerosol-α-Pinene ozonolysis, J Geophys Res-Atmos, 121, 12476-12483, 10.1002/2016jd025999, 2016.

Huang, Y., Lee, S. C., Ho, K. F., Ho, S. S. H., Cao, N. Y., Cheng, Y., and Gao, Y.: Effect of ammonia on ozone-initiated formation of indoor secondary products with emissions from cleaning products, Atmos. Environ., 59, 224-231, 10.1016/j.atmosenv.2012.04.059, 2012.

Huffman, J. A., Docherty, K. S., Mohr, C., Cubison, M. J., Ulbrich, I. M., Ziemann, P. J., Onasch, T. B., and Jimenez, J. L.: Chemically-resolved volatility measurements of organic aerosol fom different sources, Environ. Sci. Technol., 43, 5351-5357, 10.1021/es803539d, 2009.

Jang, M., Czoschke, N. M., Lee, S., and Kamens, R. M.: Heterogeneous atmospheric aerosol production by acid-catalyzed particle-phase reactions, Science, 298, 814-817, 10.1126/science.1075798, 2002.

Ji, Y., Zhao, J., Terazono, H., Misawa, K., Levitt, N. P., Li, Y., Lin, Y., Peng, J., Wang, Y., Duan, L., Pan, B., Zhang, F., Feng, X., An, T., Marrero-Ortiz, W., Secrest, J., Zhang, A. L., Shibuya, K., Molina, M. J., and Zhang, R.: Reassessing the atmospheric oxidation mechanism of toluene, Proc. Natl. Acad. Sci. U. S. A., 114, 8169-8174, 10.1073/pnas.1705463114, 2017.

Jiang, X. T., Lv, C., You, B., Liu, Z. Y., Wang, X. F., and Du, L.: Joint impact of atmospheric SO_2 and NH_3 on the formation of nanoparticles from photo-oxidation of a typical biomass burning compound, Environ Sci-Nano, 7, 2532-2545, 10.1039/d0en00520g, 2020.

Jimenez, J. L., Canagaratna, M. R., Donahue, N. M., Prevot, A. S., Zhang, Q., Kroll, J. H., DeCarlo, P. F., Allan, J. D., Coe, H., Ng, N. L., Aiken, A. C., Docherty, K. S., Ulbrich, I. M., Grieshop, A. P., Robinson, A. L., Duplissy, J., Smith, J. D., Wilson, K. R., Lanz, V. A., Hueglin, C., Sun, Y. L., Tian, J., Laaksonen, A., Raatikainen, T., Rautiainen, J., Vaattovaara, P., Ehn, M., Kulmala, M., Tomlinson, J. M., Collins, D. R., Cubison, M. J., Dunlea, E. J., Huffman, J. A., Onasch, T. B., Alfarra, M. R., Williams, P. I., Bower, K., Kondo, Y., Schneider, J., Drewnick, F., Borrmann, S., Weimer, S., Demerjian, K., Salcedo, D., Cottrell, L., Griffin, R., Takami, A., Miyoshi, T., Hatakeyama, S., Shimono, A., Sun, J. Y., Zhang, Y. M., Dzepina, K., Kimmel, J. R., Sueper, D., Jayne, J. T., Herndon, S. C., Trimborn, A. M., Williams, L. R., Wood, E. C., Middlebrook, A. M., Kolb, C. E., Baltensperger, U., and Worsnop, D. R.: Evolution of organic aerosols in the atmosphere, Science, 326, 1525-1529, 10.1126/science.1180353, 2009.

Kawamura, K., and Bikkina, S.: A review of dicarboxylic acids and related compounds in atmospheric aerosols: Molecular distributions, sources and transformation, Atmos. Res., 170, 140-160, 10.1016/j.atmosres.2015.11.018, 2016.

Kourtchev, I., Doussin, J. F., Giorio, C., Mahon, B., Wilson, E. M., Maurin, N., Pangui, E., Venables, D. S., Wenger, J. C., and Kalberer, M.: Molecular composition of fresh and aged secondary organic aerosol from a mixture of biogenic volatile compounds: a high-resolution mass spectrometry study, Atmos. Chem. Phys., 15, 5683-5695, 10.5194/acp-15-5683-2015, 2015.

Krechmer, J. E., Day, D. A., and Jimenez, J. L.: Always lost but never forgotten: Gas-phase wall losses are important in all teflon environmental chambers, Environ. Sci. Technol., 54, 12890-12897, 10.1021/acs.est.0c03381, 2020.

Kroll, J. H., Donahue, N. M., Jimenez, J. L., Kessler, S. H., Canagaratna, M. R., Wilson, K. R., Altieri, K. E., Mazzoleni, L. R., Wozniak, A. S., Bluhm, H., Mysak, E. R., Smith, J. D., Kolb, C. E., and Worsnop, D. R.: Carbon oxidation state as a metric for describing the chemistry of atmospheric organic aerosol, Nat. Chem., 3, 133-139, 10.1038/nchem.948, 2011.

Kuwata, M., and Martin, S. T.: Phase of atmospheric secondary organic material affects its reactivity, Proc. Natl. Acad. Sci. U. S. A., 109, 17354-17359, 10.1073/pnas.1209071109, 2012.

Laskin, A., Laskin, J., and Nizkorodov, S. A.: Chemistry of atmospheric brown carbon, Chem. Rev., 115, 4335-4382, 10.1021/cr5006167, 2015.

Laskin, J., Laskin, A., Roach, P. J., Slysz, G. W., Anderson, G. A., Nizkorodov, S. A., Bones, D. L., and Nguyen, L. Q.: High-resolution desorption electrospray ionization mass spectrometry for chemical characterization of organic aerosols, Anal. Chem., 82, 2048-2058, 10.1021/ac902801f, 2010.

Laskin, J., Laskin, A., Nizkorodov, S. A., Roach, P., Eckert, P., Gilles, M. K., Wang, B., Lee, H. J., and Hu, Q.: Molecular selectivity of brown carbon chromophores, Environ. Sci. Technol., 48, 12047-12055, 10.1021/es503432r, 2014.

Lee, A. K., Zhao, R., Li, R., Liggio, J., Li, S. M., and Abbatt, J. P.: Formation of light absorbing organo-

nitrogen species from evaporation of droplets containing glyoxal and ammonium sulfate, Environ. Sci. Technol., 47, 12819-12826, 10.1021/es402687w, 2013.

Li, K., Chen, L., White, S. J., Yu, H., Wu, X., Gao, X., Azzi, M., and Cen, K.: Smog chamber study of the role of NH_3 in new particle formation from photo-oxidation of aromatic hydrocarbons, Sci. Total Environ., 619-620, 927-937, 10.1016/j.scitotenv.2017.11.180, 2018.

Lian, X., Zhang, G., Yang, Y., Lin, Q., Fu, Y., Jiang, F., Peng, L., Hu, X., Chen, D., Wang, X., Peng, P. a., Sheng, G., and Bi, X.: Evidence for the formation of imidazole from carbonyls and reduced nitrogen species at the individual particle level in the ambient atmosphere, Environ. Sci. Tech. Let., 10.1021/acs.estlett.0c00722, 2020.

Liu, M., Huang, X., Song, Y., Xu, T., Wang, S., Wu, Z., Hu, M., Zhang, L., Zhang, Q., Pan, Y., Liu, X., and Zhu, T.: Rapid SO_2 emission reductions significantly increase tropospheric ammonia concentrations over the North China Plain, Atmos. Chem. Phys., 18, 17933-17943, 10.5194/acp-18-17933-2018, 2018.

Liu, S. J., Jia, L., Xu, Y., Tsona, N. T., Ge, S. S., and Du, L.: Photooxidation of cyclohexene in the presence of SO_2: SOA yield and chemical composition, Atmos. Chem. Phys., 17, 13329-13343, 10.5194/acp-17-13329-2017, 2017.

Liu, S. J., Jiang, X. T., Tsona, N. T., Lv, C., and Du, L.: Effects of NOx, SO_2 and RH on the SOA formation from cyclohexene photooxidation, Chemosphere, 216, 794-804, 10.1016/j.chemosphere.2018.10.180, 2019a.

Liu, S. J., Tsona, N. T., Zhang, Q., Jia, L., Xu, Y. F., and Du, L.: Influence of relative humidity on cyclohexene SOA formation from OH photooxidation, Chemosphere, 231, 478-486, 10.1016/j.chemosphere.2019.05.131, 2019b.

Liu, S. J., Wang, Y., Wang, G., Zhang, S., Li, D., Du, L., Wu, C., Du, W., and Ge, S.: Enhancing effect of NO_2 on the formation of light-absorbing secondary organic aerosols from toluene photooxidation, Sci. Total Environ., 794, 148714, 10.1016/j.scitotenv.2021.148714, 2021.

Liu, Y. C., Liggio, J., Staebler, R., and Li, S. M.: Reactive uptake of ammonia to secondary organic aerosols: Kinetics of organonitrogen formation, Atmos. Chem. Phys., 15, 13569-13584, 10.5194/acp-15-13569-2015, 2015.

Ma, P., Zhang, P., Shu, J., Yang, B., and Zhang, H.: Characterization of secondary organic aerosol from photo-oxidation of gasoline exhaust and specific sources of major components, Environ. Pollut., 232, 65-72, 10.1016/j.envpol.2017.09.018, 2018a.

Ma, Q., Lin, X., Yang, C., Long, B., Gai, Y., and Zhang, W.: The influences of ammonia on aerosol formation in the ozonolysis of styrene: Roles of Criegee intermediate reactions, R. Soc. Open Sci., 5, 172171, 10.1098/rsos.172171, 2018b.

Malecha, K. T., and Nizkorodov, S. A.: Photodegradation of secondary organic aerosol particles as a source of small, oxygenated volatile organic compounds, Environ. Sci. Technol., 50, 9990-9997, 10.1021/acs.est.6b02313, 2016.

Mandariya, A. K., Gupta, T., and Tripathi, S. N.: Effect of aqueous-phase processing on the formation and evolution of organic aerosol (OA) under different stages of fog life cycles, Atmos. Environ., 206, 60-71, 10.1016/j.atmosenv.2019.02.047, 2019.

Middlebrook, A. M., Bahreini, R., Jimenez, J. L., and Canagaratna, M. R.: Evaluation of composition-dependent collection efficiencies for the aerodyne aerosol mass spectrometer using field data, Aerosol Sci. Tech., 46, 258-271, 10.1080/02786826.2011.620041, 2012.

Moise, T., Flores, J. M., and Rudich, Y.: Optical properties of secondary organic aerosols and their changes by chemical processes, Chem. Rev., 115, 4400-4439, 10.1021/cr5005259, 2015.

Na, K., Song, C., Switzer, C., and Cocker, D. R.: Effect of ammonia on secondary organic aerosol formation from α-pinene ozonolysis in dry and humid conditions, Environ. Sci. Technol., 41, 6096-6102, 10.1021/es061956y, 2007.

Ng, N. L., Chhabra, P. S., Chan, A. W. H., Surratt, J. D., Kroll, J. H., Kwan, A. J., McCabe, D. C.,

751 Wennberg, P. O., Sorooshian, A., Murphy, S. M., Dalleska, N. F., Flagan, R. C., and Seinfeld, J. H.:
752 Effect of NOx level on secondary organic aerosol (SOA) formation from the photooxidation of
753 terpenes, Atmos. Chem. Phys., 7, 5159-5174, 10.5194/acp-7-5159-2007, 2007a.

754 Ng, N. L., Kroll, J. H., Chan, A. W. H., Chhabra, P. S., Flagan, R. C., and Seinfeld, J. H.: Secondary
755 organic aerosol formation from m-xylene, toluene, and benzene, Atmos. Chem. Phys., 7, 3909-3922,
756 10.5194/acp-7-3909-2007, 2007b.

757 Ng, N. L., Canagaratna, M. R., Zhang, Q., Jimenez, J. L., Tian, J., Ulbrich, I. M., Kroll, J. H., Docherty,
758 K. S., Chhabra, P. S., Bahreini, R., Murphy, S. M., Seinfeld, J. H., Hildebrandt, L., Donahue, N. M.,
759 DeCarlo, P. F., Lanz, V. A., Prévôt, A. S. H., Dinar, E., Rudich, Y., and Worsnop, D. R.: Organic
760 aerosol components observed in Northern Hemispheric datasets from Aerosol Mass Spectrometry,
761 Atmos. Chem. Phys., 10, 4625-4641, 10.5194/acp-10-4625-2010, 2010.

762 Ng, N. L., Brown, S. S., Archibald, A. T., Atlas, E., Cohen, R. C., Crowley, J. N., Day, D. A., Donahue,
763 N. M., Fry, J. L., Fuchs, H., Griffin, R. J., Guzman, M. I., Herrmann, H., Hodzic, A., Iinuma, Y.,
764 Jimenez, J. L., Kiendler-Scharr, A., Lee, B. H., Luecken, D. J., Mao, J., McLaren, R., Mutzel, A.,
765 Osthoff, H. D., Ouyang, B., Picquet-Varrault, B., Platt, U., Pye, H. O. T., Rudich, Y., Schwantes, R.
766 H., Shiraiwa, M., Stutz, J., Thornton, J. A., Tilgner, A., Williams, B. J., and Zaveri, R. A.: Nitrate
767 radicals and biogenic volatile organic compounds: Oxidation, mechanisms, and organic aerosol,
768 Atmos. Chem. Phys., 17, 2103-2162, 10.5194/acp-17-2103-2017, 2017.

769 Nguyen, T. B., Laskin, A., Laskin, J., and Nizkorodov, S. A.: Brown carbon formation from
770 ketoaldehydes of biogenic monoterpenest, Faraday Discuss., 165, 473-494, 10.1039/c3fd00036b,
771 2013.

772 NIST: NIST Chemistry WebBook Standard Reference Database 69, https://doi.org/10.18434/T4D303,
773 2020.

774 Noziere, B., Dziedzic, P., and Cordova, A.: Products and kinetics of the liquid-phase reaction of glyoxal
775 catalyzed by ammonium ions (NH_4^+), J. Phys. Chem. A, 113, 231-237, 10.1021/jp8078293, 2009.

776 Ortiz-Montalvo, D. L., Hakkinen, S. A., Schwier, A. N., Lim, Y. B., McNeill, V. F., and Turpin, B. J.:
777 Ammonium addition (and aerosol pH) has a dramatic impact on the volatility and yield of glyoxal
778 secondary organic aerosol, Environ. Sci. Technol., 48, 255-262, 10.1021/es4035667, 2014.

779 Paciga, A. L., Riipinen, I., and Pandis, S. N.: Effect of ammonia on the volatility of organic diacids,
780 Environ. Sci. Technol., 48, 13769-13775, 10.1021/es5037805, 2014.

781 Pathak, R. K., Stanier, C. O., Donahue, N. M., and Pandis, S. N.: Ozonolysis of alpha-pinene at
782 atmospherically relevant concentrations: Temperature dependence of aerosol mass fractions (yields),
783 J Geophys Res-Atmos, 112, Artn D03201, 10.1029/2006jd007436, 2007.

784 Peng, C., Yang, F., Tian, M., Shi, G., Li, L., Huang, R. J., Yao, X., Luo, B., Zhai, C., and Chen, Y.: Brown
785 carbon aerosol in two megacities in the Sichuan Basin of southwestern China: Light absorption
786 properties and implications, Sci. Total Environ., 719, 137483, 10.1016/j.scitotenv.2020.137483,
787 2020.

788 Prinn, R. G., Weiss, R. F., Miller, B. R., Huang, J., Alyea, F. N., Cunnold, D. M., Fraser, P. J., Hartley, D.
789 E., and Simmonds, P. G.: Atmospheric trends and lifetime of CH_3CCl_3 and global OH
790 concentrations, Science, 269, 187-192, 10.1126/science.269.5221.187, 1995.

791 Qi, X., Zhu, S., Zhu, C., Hu, J., Lou, S., Xu, L., Dong, J., and Cheng, P.: Smog chamber study of the
792 effects of NOx and NH_3 on the formation of secondary organic aerosols and optical properties from
793 photo-oxidation of toluene, Sci. Total Environ., 727, 138632, 10.1016/j.scitotenv.2020.138632,
794 2020.

795 Sarrafzadeh, M., Wildt, J., Pullinen, I., Springer, M., Kleist, E., Tillmann, R., Schmitt, S. H., Wu, C.,
796 Mentel, T. F., Zhao, D. F., Hastie, D. R., and Kiendler-Scharr, A.: Impact of NOx and OH on
797 secondary organic aerosol formation from β-pinene photooxidation, Atmos. Chem. Phys., 16,
798 11237-11248, 10.5194/acp-16-11237-2016, 2016.

799 Sun, Y. L., Zhang, Q., Schwab, J. J., Demerjian, K. L., Chen, W. N., Bae, M. S., Hung, H. M., Hogrefe,
800 O., Frank, B., Rattigan, O. V., and Lin, Y. C.: Characterization of the sources and processes of
801 organic and inorganic aerosols in New York city with a high-resolution time-of-flight aerosol mass

apectrometer, Atmos. Chem. Phys., 11, 1581-1602, 10.5194/acp-11-1581-2011, 2011.

Surratt, J. D., Murphy, S. M., Kroll, J. H., Ng, N. L., Hildebrandt, L., Sorooshian, A., Szmigielski, R., Vermeylen, R., Maenhaut, W., Claeys, M., Flagan, R. C., and Seinfeld, J. H.: Chemical composition of secondary organic aerosol formed from the photooxidation of isoprene, J. Phys. Chem. A, 110, 9665-9690, 10.1021/jp061734m, 2006.

Volkamer, R., Jimenez, J. L., San Martini, F., Dzepina, K., Zhang, Q., Salcedo, D., Molina, L. T., Worsnop, D. R., and Molina, M. J.: Secondary organic aerosol formation from anthropogenic air pollution: Rapid and higher than expected, Geophys. Res. Lett., 33, Artn L17811, 10.1029/2006gl026899, 2006.

Vu, T. V., Shi, Z., Cheng, J., Zhang, Q., He, K., Wang, S., and Harrison, R. M.: Assessing the impact of clean air action on air quality trends in Beijing using a machine learning technique, Atmos. Chem. Phys., 19, 11303-11314, 10.5194/acp-19-11303-2019, 2019.

Wang, G., Zhang, F., Peng, J., Duan, L., Ji, Y., Marrero-Ortiz, W., Wang, J., Li, J., Wu, C., Cao, C., Wang, Y., Zheng, J., Secrest, J., Li, Y., Wang, Y., Li, H., Li, N., and Zhang, R.: Particle acidity and sulfate production during severe haze events in China cannot be reliably inferred by assuming a mixture of inorganic salts, Atmos. Chem. Phys., 18, 10123-10132, 10.5194/acp-18-10123-2018, 2018a.

Wang, G. H., Zhang, R. Y., Gomez, M. E., Yang, L. X., Zamora, M. L., Hu, M., Lin, Y., Peng, J. F., Guo, S., Meng, J. J., Li, J. J., Cheng, C. L., Hu, T. F., Ren, Y. Q., Wang, Y. S., Gao, J., Cao, J. J., An, Z. S., Zhou, W. J., Li, G. H., Wang, J. Y., Tian, P. F., Marrero-Ortiz, W., Secrest, J., Du, Z. F., Zheng, J., Shang, D. J., Zeng, L. M., Shao, M., Wang, W. G., Huang, Y., Wang, Y., Zhu, Y. J., Li, Y. X., Hu, J. X., Pan, B., Cai, L., Cheng, Y. T., Ji, Y. M., Zhang, F., Rosenfeld, D., Liss, P. S., Duce, R. A., Kolb, C. E., and Molina, M. J.: Persistent sulfate formation from London Fog to Chinese haze, Proc. Natl. Acad. Sci. U. S. A., 113, 13630-13635, 10.1073/pnas.1616540113, 2016.

Wang, R. Y., Ye, X. N., Liu, Y. X., Li, H. W., Yang, X., Chen, J. M., Gao, W., and Yin, Z.: Characteristics of atmospheric ammonia and its relationship with vehicle emissions in a megacity in China, Atmos. Environ., 182, 97-104, 10.1016/j.atmosenv.2018.03.047, 2018b.

Wang, S. W., Zhang, Q., Martin, R. V., Philip, S., Liu, F., Li, M., Jiang, X. T., and He, K. B.: Satellite measurements oversee China's sulfur dioxide emission reductions from coal-fired power plants, Environ. Res. Lett., 10, 114015, 10.1088/1748-9326/10/11/114015, 2015.

Wang, X., Gao, S., Yang, X., Chen, H., Chen, J., Zhuang, G., Surratt, J. D., Chan, M. N., and Seinfeld, J. H.: Evidence for high molecular weight nitrogen-containing organic salts in urban aerosols, Environ. Sci. Technol., 44, 4441-4446, 10.1021/es1001117, 2010.

Wang, Y., Chen, Y., Wu, Z., Shang, D., Bian, Y., Du, Z., Schmitt, S. H., Su, R., Gkatzelis, G. I., Schlag, P., Hohaus, T., Voliotis, A., Lu, K., Zeng, L., Zhao, C., Alfarra, M. R., McFiggans, G., Wiedensohler, A., Kiendler-Scharr, A., Zhang, Y., and Hu, M.: Mutual promotion between aerosol particle liquid water and particulate nitrate enhancement leads to severe nitrate-dominated particulate matter pollution and low visibility, Atmos. Chem. Phys., 20, 2161-2175, 10.5194/acp-20-2161-2020, 2020.

Wu, C., Zhang, S., Wang, G., Lv, S., Li, D., Liu, L., Li, J., Liu, S., Du, W., Meng, J., Qiao, L., Zhou, M., Huang, C., and Wang, H.: Efficient heterogeneous formation of ammonium nitrate on the saline mineral particle surface in the atmosphere of east asia during dust storm periods, Environ. Sci. Technol., 54, 15622-15630, 10.1021/acs.est.0c04544, 2020.

Xia, Y., Zhao, Y., and Nielsen, C. P.: Benefits of China's efforts in gaseous pollutant control indicated by the bottom-up emissions and satellite observations 2000-2014, Atmos. Environ., 136, 43-53, 10.1016/j.atmosenv.2016.04.013, 2016.

Xie, M., Chen, X., Hays, M. D., Lewandowski, M., Offenberg, J., Kleindienst, T. E., and Holder, A. L.: Light absorption of secondary organic aerosol: Composition and contribution of nitroaromatic compounds, Environ. Sci. Technol., 51, 11607-11616, 10.1021/acs.est.7b03263, 2017.

Xu, J., Huang, M. Q., Cai, S. Y., Liao, Y. M., Hu, C. J., Zhao, W. X., Gu, X. J., and Zhang, W. J.: Chemical composition and reaction mechanisms for aged p-xylene secondary organic aerosol in the presence of ammonia, J. Chin. Chem. Soc., 65, 578-590, 10.1002/jccs.201700249, 2018.

Xu, L., Kollman, M. S., Song, C., Shilling, J. E., and Ng, N. L.: Effects of NOx on the volatility of

secondary organic aerosol from isoprene photooxidation, Environ. Sci. Technol., 48, 2253-2262, 10.1021/es404842g, 2014.

Xu, L., Moller, K. H., Crounse, J. D., Kjaergaard, H. G., and Wennberg, P. O.: New insights into the radical chemistry and product distribution in the OH-initiated oxidation of benzene, Environ. Sci. Technol., 54, 13467-13477, 10.1021/acs.est.0c04780, 2020.

Yang, W. Y., Li, J., Wang, M., Sun, Y. L., and Wang, Z. F.: A case study of investigating secondary organic aerosol formation pathways in beijing using an observation-based SOA box model, Aerosol Air Qual. Res., 18, 1606-1616, 10.4209/aaqr.2017.10.0415, 2018.

Yang, Y., Vance, M., Tou, F. Y., Tiwari, A., Liu, M., and Hochella, M. F.: Nanoparticles in road dust from impervious urban surfaces: Distribution, identification, and environmental implications, Environ Sci-Nano, 3, 534-544, 10.1039/c6en00056h, 2016.

Yang, Z., Tsona, N. T., Li, J., Wang, S., Xu, L., You, B., and Du, L.: Effects of NOx and SO_2 on the secondary organic aerosol formation from the photooxidation of 1,3,5-trimethylbenzene: A new source of organosulfates, Environ. Pollut., 264, 114742, 10.1016/j.envpol.2020.114742, 2020.

Zhang, L., Wang, Y., Feng, C., Liang, S., Liu, Y., Du, H., and Jia, N.: Understanding the industrial NOx and SO_2 pollutant emissions in China from sector linkage perspective, Sci. Total Environ., 770, 145242, 10.1016/j.scitotenv.2021.145242, 2021a.

Zhang, Q., Jimenez, J. L., Canagaratna, M. R., Ulbrich, I. M., Ng, N. L., Worsnop, D. R., and Sun, Y.: Understanding atmospheric organic aerosols via factor analysis of aerosol mass spectrometry: a review, Anal. Bioanal. Chem., 401, 3045-3067, 10.1007/s00216-011-5355-y, 2011.

Zhang, R., Wang, G., Guo, S., Zamora, M. L., Ying, Q., Lin, Y., Wang, W., Hu, M., and Wang, Y.: Formation of urban fine particulate matter, Chem. Rev., 115, 3803-3855, 10.1021/acs.chemrev.5b00067, 2015a.

Zhang, S., Li, D., Ge, S., Liu, S., Wu, C., Wang, Y., Chen, Y., Lv, S., Wang, F., Meng, J., and Wang, G.: Rapid sulfate formation from synergetic oxidation of SO_2 by O_3 and NO_2 under ammonia-rich conditions: Implications for the explosive growth of atmospheric $PM_{2.5}$ during haze events in China, Sci. Total Environ., 772, 144897, 10.1016/j.scitotenv.2020.144897, 2021b.

Zhang, X., Cappa, C. D., Jathar, S. H., McVay, R. C., Ensberg, J. J., Kleeman, M. J., and Seinfeld, J. H.: Influence of vapor wall loss in laboratory chambers on yields of secondary organic aerosol, Proc. Natl. Acad. Sci. U. S. A., 111, 5802-5807, 10.1073/pnas.1404727111, 2014.

Zhang, X., Schwantes, R. H., McVay, R. C., Lignell, H., Coggon, M. M., Flagan, R. C., and Seinfeld, J. H.: Vapor wall deposition in Teflon chambers, Atmos. Chem. Phys., 15, 4197-4214, 10.5194/acp-15-4197-2015, 2015b.

Zhao, D. F., Schmitt, S. H., Wang, M. J., Acir, I. H., Tillmann, R., Tan, Z. F., Novelli, A., Fuchs, H., Pullinen, I., Wegener, R., Rohrer, F., Wildt, J., Kiendler-Scharr, A., Wahner, A., and Mentel, T. F.: Effects of NOx and SO_2 on the secondary organic aerosol formation from photooxidation of α-pinene and limonene, Atmos. Chem. Phys., 18, 1611-1628, 10.5194/acp-18-1611-2018, 2018.

Zou, Y., Deng, X. J., Zhu, D., Gong, D. C., Wang, H., Li, F., Tan, H. B., Deng, T., Mai, B. R., Liu, X. T., and Wang, B. G.: Characteristics of 1 year of observational data of VOCs, NOx and O_3 at a suburban site in Guangzhou, China, Atmos. Chem. Phys., 15, 6625-6636, 10.5194/acp-15-6625-2015, 2015.

Tables

Table 1. Summary of experimental conditions in this study

No.	Tol_0 (ppb)	ΔTol (ppb)	NH_3[a] (ppb)	NO_2 (ppb)	RH (%)	SOA mass conc.[b,c] (μg m^{-3})	SOA yield[b] (%)
Exp.1	664.1	551.2	-	-	25 ± 1	637 ± 14.6	28.1
Exp.2	618.7	499.4	~200	-	23 ± 1	867 ± 12.7	34.7
Exp.3	620.9	526.1	~200	62	26 ± 1	1020 ± 10.6	42.7
Exp.4	645.7	539.5	-	63	25 ± 1	452 ± 18.9	19.5

[a] The concentration of NH_3 is estimated by the amount of NH_3 added and the volume of the smog chamber. [b] SOA concentration and yield were calculated after taking into account the wall loss. [c] The reported SOA mass concentrations was the peak values after the wall loss correction.

Figures

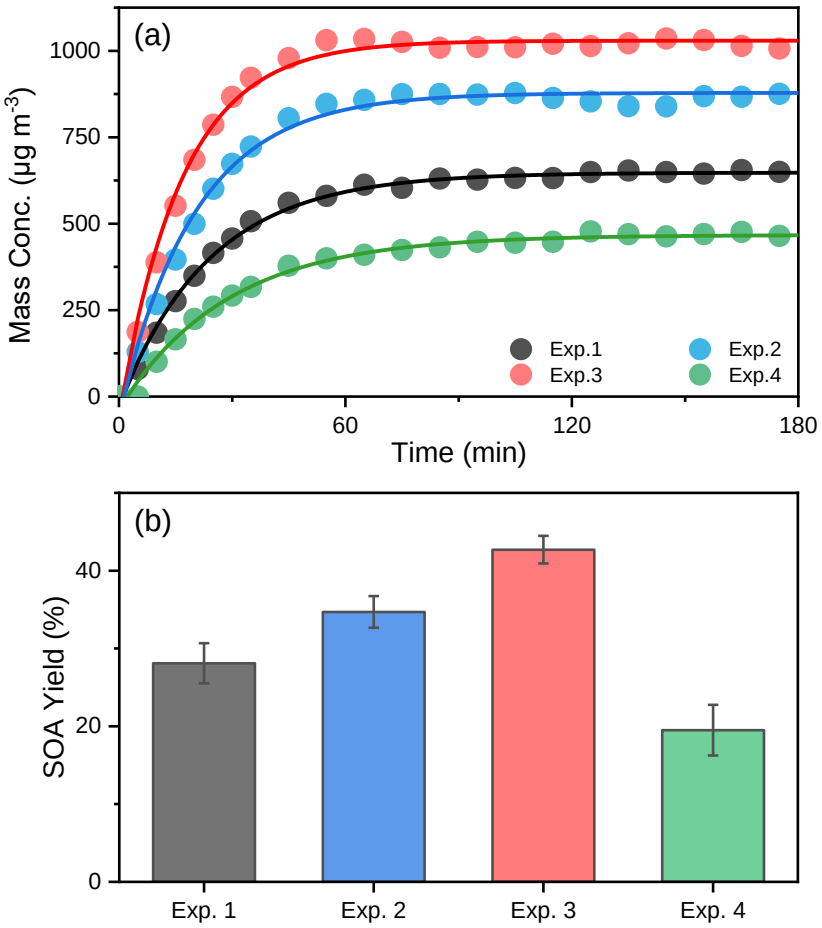

Fig. 1. The evolution of mass concentration (a) and yield (b) of toluene-derived SOA in different experiments. All the mass concentrations were wall-loss corrected. The error bars were calculated by the fluctuation of measured SOA concentration after the UV light was turn off at the end of each experiment

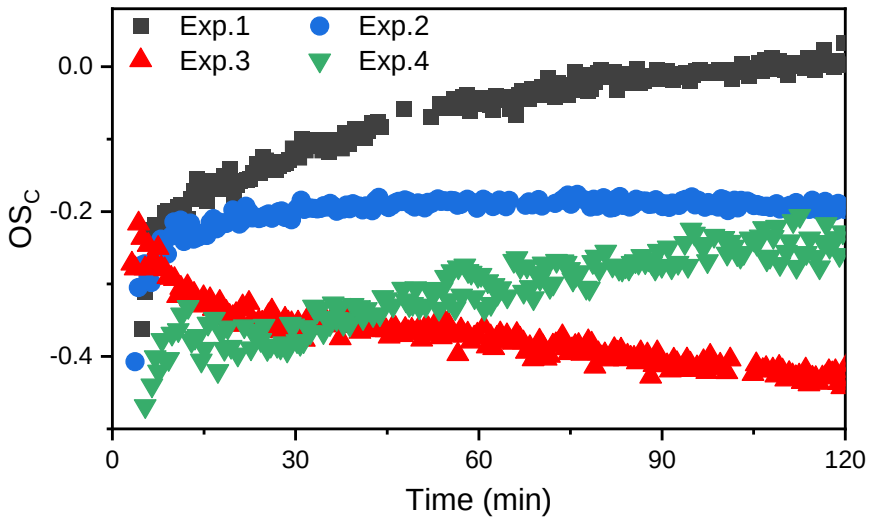

Fig. 2. The OS_C values for the toluene SOA formed under different NH_3/NOx conditions.

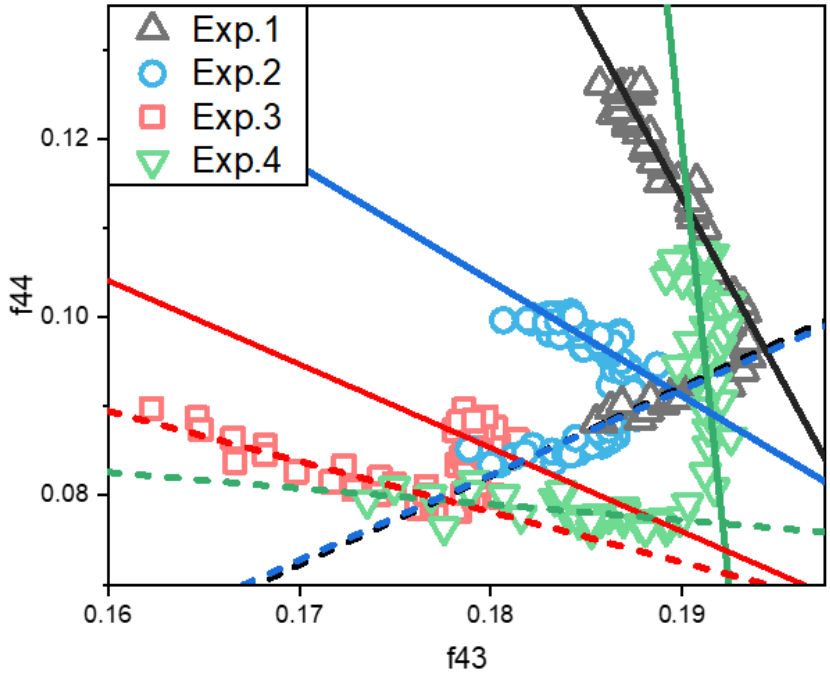

Fig. 3. The relationship between total organic signals at 43 m/z (f43) *vs.* 44 m/z (f44) from SOA data during the photooxidation process. The f43 *vs.* f44 plots exhibited inflection points during the photooxidation process. The dashed lines indicate the trends of f43 *vs.* f44 for the SOA formation stage (before the inflection point) and the solid lines for the stable stage.

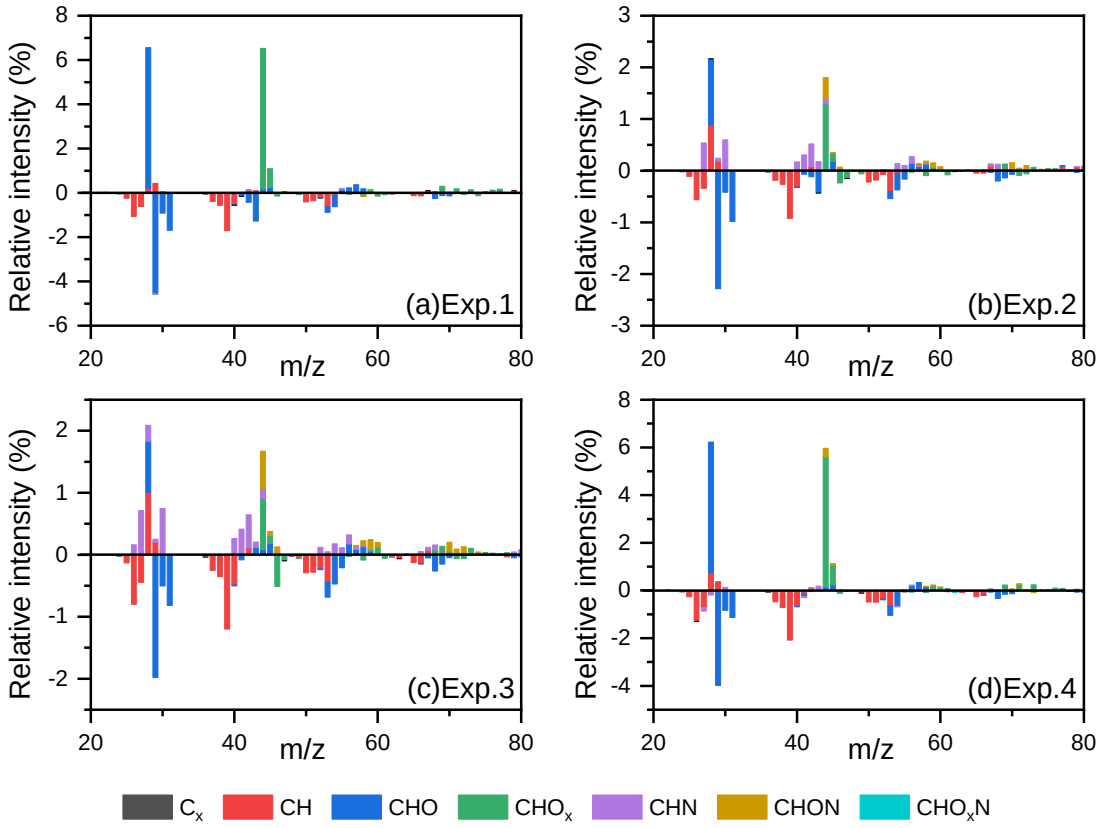

Fig. 4. The differential spectra of toluene SOA in the formation and stable stages. Data were taken and analyzed at a high resolution but were summarized to a unit mass resolution for display. Only minimal N-containing fragments could be observed in the Exp.1 without added NH_3 and NOx. These N-containing fragments could be attributed to the background NH_3 and NOx in the chamber or the systematic errors from AMS.

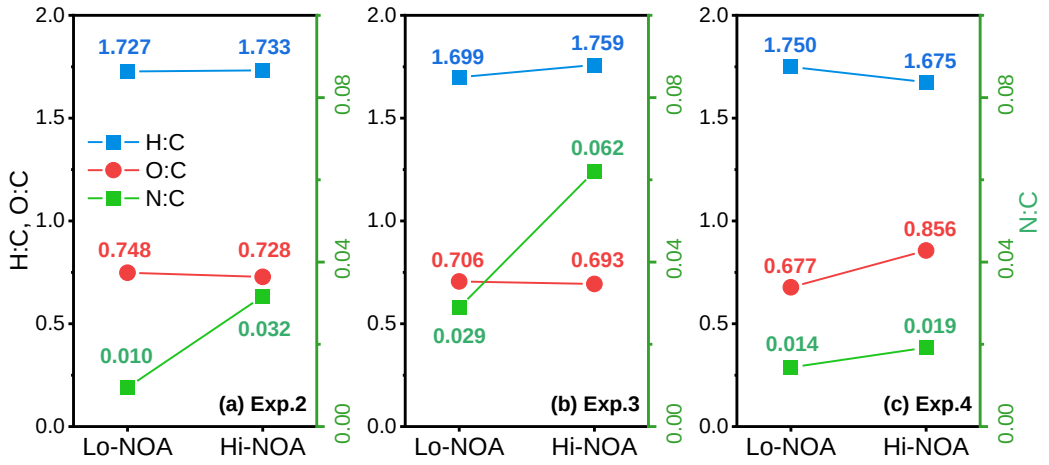

928

929 **Fig. 5.** The H/C, O/C, and N/C values of Hi-NOA and Lo-NOA for each experiment. (a) Exp. 2
930 with 200 ppb NH_3, (b) Exp. 3 with 200 ppb NH_3 and 62 ppb NO_2, and (c) Exp. 4 with 63 ppb
931 NO_2.

932

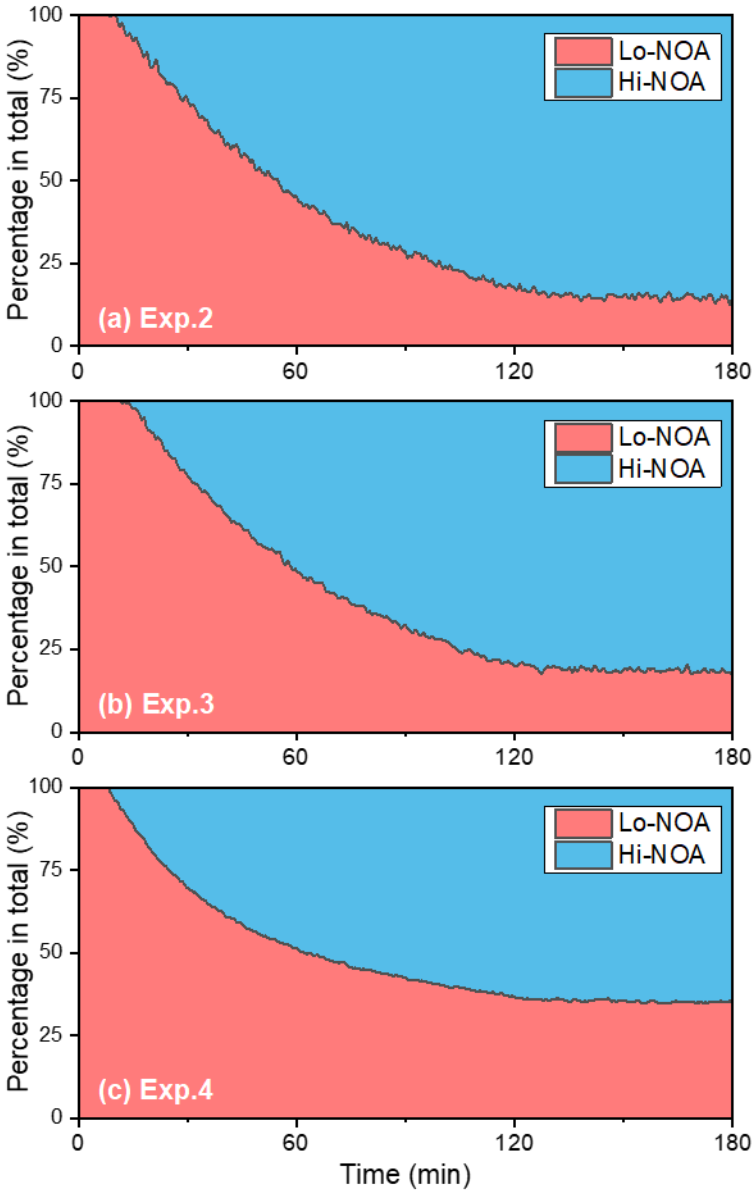

Fig. 6. The evolution of high-nitrogen OA (Hi-NOA) and low-nitrogen OA (Lo-NOA) during the photooxidation process under different NOx/NH_3 concentrations. Hi-NOA and Lo-NOA were not consistent among experiments. (a) Exp. 2 with 200 ppb NH_3, (b) Exp. 3 with 200 ppb NH_3 and 62 ppb NO_2, and (c) Exp. 4 with 63 ppb NO_2.

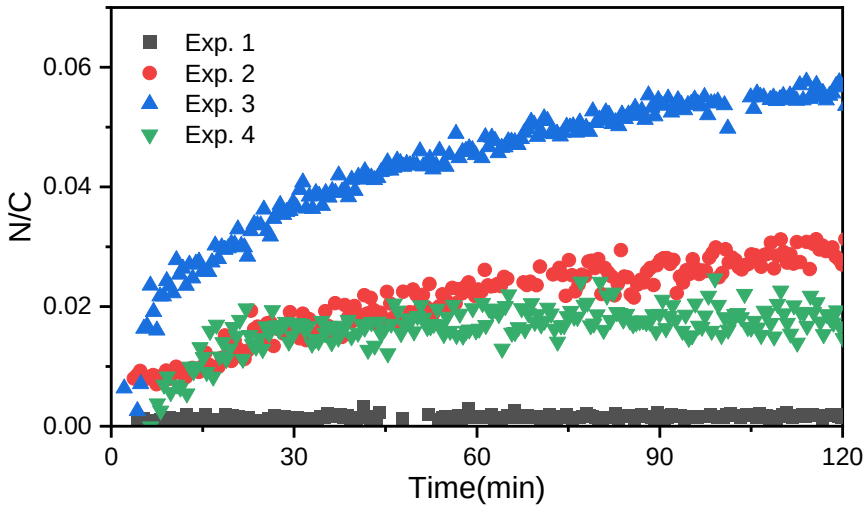

939

940 **Fig. 7.** The evolution of N/C in different experiments.

941

942

943

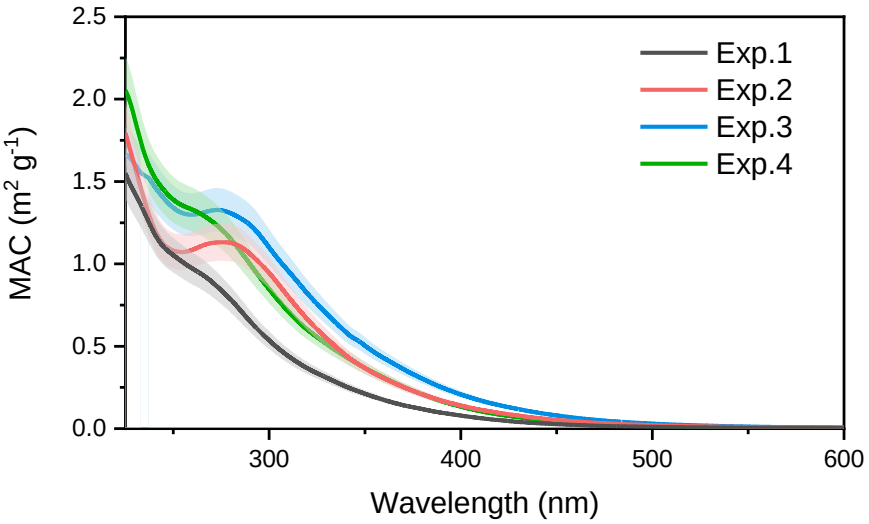

944

945 **Fig. 8.** The MAC over the range of 230 – 600 nm for the toluene SOA formed under different
946 experiment conditions.

947